

## **Sb<sub>2</sub>Se<sub>3</sub>: a possible future for thin-film photovoltaics?**

G. SPAGGIARI(\*)

*Dipartimento di Scienze Matematiche, Fisiche e Informatiche,  
Università di Parma - Parma, Italy*

*Istituto dei Materiali per l'Elettronica ed il Magnetismo, CNR - Parma, Italy*

S. RAMPINO

*Istituto dei Materiali per l'Elettronica ed il Magnetismo, CNR - Parma, Italy*

D. BERSANI

*Dipartimento di Scienze Matematiche,  
Fisiche e Informatiche, Università di Parma - Parma, Italy*

**Summary.** — Antimony selenide (Sb<sub>2</sub>Se<sub>3</sub>) is today one of the most promising alternative materials for p-type absorbers in thin-film photovoltaics, with an optimal band-gap and a very high absorption coefficient. However, its crystal structure is extremely anisotropic and its natural carrier density is generally very low. Sb<sub>2</sub>Se<sub>3</sub> thin films have been deposited by two different high-energy techniques: magnetron RF-sputtering (MS) and low-temperature pulsed electron deposition (LT-PED). Their dominant crystallographic orientations have been studied as a function of deposition parameters and of the different used substrates, while complete solar cells have been subsequently made with the obtained samples to confirm the dependence of conversion efficiencies on the observed (Sb<sub>4</sub>Se<sub>6</sub>)<sub>n</sub> ribbon orientation. Cu-doped Sb<sub>2</sub>Se<sub>3</sub> thin-films have been also preliminary prepared in order to evaluate a possible route to further improve the free charge-carrier density and the cell performance.

---

(\*) Corresponding author. E-mail: [giulia.spaggiari1@unipr.it](mailto:giulia.spaggiari1@unipr.it)

## 1. – Introduction

Today the world is in strong need of economic and efficient renewable energy sources. While commercial silicon-based solar panels are already available for large-scale photovoltaic energy production, at lower and lower cost and with efficiencies closer and closer to the maximum theoretical value, thin-film solar cells are instead making their way in the parallel growing markets of building-integrated photovoltaics, semitransparent and bi-facial solar panels, flexible and/or light-weight applications. The leading materials in thin-film photovoltaics are today amorphous-silicon (a-Si), cadmium telluride (CdTe) and copper-indium-gallium selenide (CIGS), but each of them has a weakness: efficiency of a-Si modules is languishing since several years between 11 and 12% [1]; CdTe modules sales are threatened by the carcinogenicity of cadmium-related compounds after decomposition [2], despite their good efficiency and solid production process; CIGS modules are more expensive than the other two because of the high prices of indium and gallium [3]. For all these reasons, in the last years researcher are intensively seeking for possible alternative absorber materials to be exploited in thin-film solar cells, possibly featuring high efficiency, low toxicity, and low competitive cost, all at the same time.

Antimony selenide ( $\text{Sb}_2\text{Se}_3$ ) is currently one of the most studied materials for this purpose. It is indeed characterized by very promising physical properties: a 1.22 eV direct band gap (1.03 eV indirect) [4], a very high density of states in the proximity of the valence band maximum, a very high absorption coefficient (more than  $10^5 \text{ cm}^{-1}$ ) [5], and a 32.2% theoretical power conversion efficiency (PCE) limit (calculated by the Shockley-Queisser model) [6]. At the same time, other properties are strongly related to its highly anisotropic crystal structure, dominated by 1D ribbons made of ( $\text{Sb}_4\text{Se}_6$ ) stacked units along the  $c$ -axis of the orthorhombic cell ( $Pbnm$  space group symmetry,  $a = 11.62 \text{ \AA}$ ,  $b = 11.77 \text{ \AA}$ ,  $c = 3.962 \text{ \AA}$ ), as clearly visible in fig. 1. Within each ribbon covalent bonds are present, while van der Waals forces are predominant between different ribbons. So, for example, hole mobility drops from  $42 \text{ cm}^2\text{V}^{-1}\text{s}^{-1}$  to  $0.7 \text{ cm}^2\text{V}^{-1}\text{s}^{-1}$  when the charge motion direction is changed from along the  $c$ -axis to along a perpendicular one [7]. This means that arranging these ribbons perpendicular to the substrate, in order to maximize the carrier transport properties, is a key challenge in the deposition of  $\text{Sb}_2\text{Se}_3$  thin films for photovoltaic applications. Once researchers focused on this goal, PCE values reported in the literature rapidly grew from less than 1% to 10% [5, 8].

In this work we report the comparison between different  $\text{Sb}_2\text{Se}_3$  thin films, deposited by two different high-energy techniques: low-temperature pulsed electron deposition (LT-PED) and Magnetron RF-Sputtering (MS). The process parameters and the substrates that produced the films with the best average crystallographic orientation are here highlighted. Complete cell structures were also realized with some of the deposited thin films and the cells performance was then correlated to the previously observed crystallographic properties. Finally, preliminary results on the production of Cu-doped  $\text{Sb}_2\text{Se}_3$  thin films are also reported and discussed, in order to assess the effects of a possible increase in the charge carrier density, which is intrinsically low in this material.

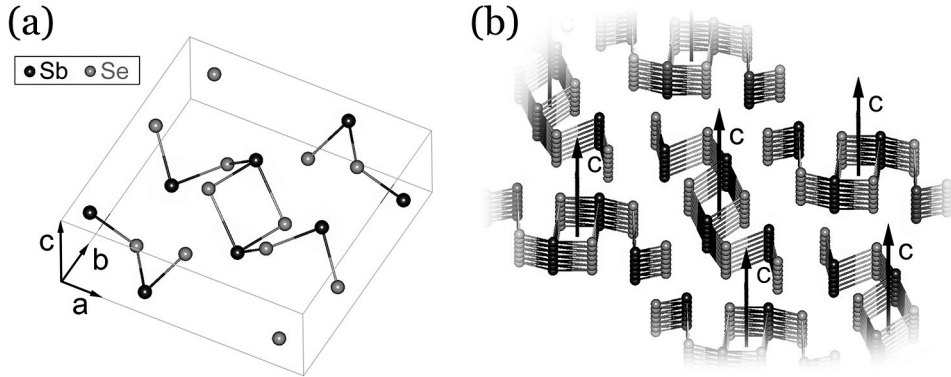


Fig. 1. – Crystal structure of  $\text{Sb}_2\text{Se}_3$  is characterized by an orthorhombic cell in the  $Pbnm$  space group: (a) unit cell; (b)  $(\text{Sb}_4\text{Se}_6)$  ribbons visualization, here obtained by the stacking of  $n = 6$  planes along the  $c$ -axis.

## 2. – Experimental

$\text{Sb}_2\text{Se}_3$  thin films were deposited using both LT-PED and MS techniques. At first, bare soda-lime glass was used to determine the best growth conditions for  $\text{Sb}_2\text{Se}_3$  crystallization, using different substrate temperatures: between  $200^\circ\text{C}$  and  $400^\circ\text{C}$  for LT-PED and between  $50^\circ\text{C}$  and  $330^\circ\text{C}$  for MS. Other parameters were previously optimized and reported (see ref. [9] for LT-PED and ref. [10] for MS). Then, depositions were also performed with both techniques on different substrates, *i.e.* molybdenum (Mo), fluorine tin oxide (FTO), cadmium sulfide on FTO (CdS/FTO), and undoped zinc oxide (ZnO), at  $300^\circ\text{C}$  to verify how crystallization was influenced by them.

The structural properties of the obtained films, with a special focus on preferential orientations, were characterized by a X-ray diffraction system (XRD, Siemens D500), in Bragg-Brentano geometry and with  $\text{CuK}\alpha$  radiation. Morphology and composition were instead controlled by a field-emission gun scanning electron microscope (FESEM-FIB, Zeiss Auriga Compact) equipped with an energy dispersive X-ray spectrometer (EDX, Oxford) optimized with a Co standard. The current density *vs.* voltage ( $J$ - $V$ ) characteristics of the solar cells were instead measured under standard test conditions (solar simulator, ABET SUN 2000) by means of a multimeter (Keithley 2614B).

## 3. – Results and discussion

Both LT-PED and MS are high-energy techniques that can be successfully employed in the deposition of  $\text{Sb}_2\text{Se}_3$  thin films. We previously demonstrated that LT-PED can be successfully used for the deposition of different layers for photovoltaic applications [9, 11-14], while MS is widely recognized as one of the leading techniques in industrial applications. The use of high-energy techniques generally enables the use of

low temperatures for the substrates, because the generated ions have enough energy to move and/or rearrange on the substrate surface, hence resulting in a good crystallization without the need of high-temperature kinetic energy. This is a very important request when industrial application is considered and/or temperature sensitive substrates are used (glass, polymers, etc.).

In the following analysis we are going to address the effect of deposition conditions on thin-films quality in terms of “good” or “bad” preferential crystalline orientations of their grains. Since charge transfer is much better along the  $(\text{Sb}_4\text{Se}_6)_n$  ribbons, the best possible preferential crystalline orientation for thin-film solar cells is the one providing vertically aligned ribbons on the substrate (*i.e.*, when  $00l$  peaks are dominant in XRD spectra), while the worst preferential crystalline orientation is the one with ribbons lying on the substrate (*i.e.*, when  $hk0$  peaks are dominant in XRD spectra). Generally also ribbons oriented along an intermediate  $(hkl)$  crystalline direction with  $l \neq 0$  and a high inclination angle to the substrate plane are considered “good”, because also in that case charge carriers can run through a rather short oblique path towards the cell contacts.

Then the obtained structural results are compared with the performance of photovoltaic cells made with some of the deposited  $\text{Sb}_2\text{Se}_3$  thin films.

**3'1. Crystallization vs. temperature.** – The effect of substrate temperature on  $\text{Sb}_2\text{Se}_3$  films crystallization was controlled at first on bare glass substrates, in order to exclude any effect due to the presence of a matching/unmatching templating lattice. The XRD spectra of selected films are reported in fig. 2 to highlight the main results.

Thin films deposited by LT-PED have a poor crystallization below  $200^\circ\text{C}$ , which then improves with increasing temperature. However, while at  $300^\circ\text{C}$  films with a partially “good” orientation are obtained, at higher temperature “bad” orientations become dominant (fig. 2(a)). On the contrary, thin-films deposited by MS crystallize above  $80^\circ\text{C}$  but start to have grains with “good” orientation only above  $260^\circ\text{C}$  (fig. 2(b)). At higher temperature ( $> 330^\circ\text{C}$ ), and for long deposition times, SEM imaging revealed the formation of elongated nano/micro-wires over the surface [10], which may be interesting for the realization of 3D cell structures, but not desired for this study.

Hence, a common substrate temperature of  $300^\circ\text{C}$  was chosen as the best one to make comparisons between the two techniques and the films obtained on a different type of substrates.

**3'2. Crystallization vs. substrate.** – Since the substrate texture and lattice can act as a template, that favours different crystallizations, the average preferential crystalline orientation was compared for  $\text{Sb}_2\text{Se}_3$  films that were deposited at  $300^\circ\text{C}$  on different substrates. In order to simplify the comparison, the following values can be defined [9]:

$$(1a) \quad TC(hkl) = n \times \frac{\frac{I(hkl)}{I_0(hkl)}}{\sum_n \frac{I(hkl)_n}{I_0(hkl)_n}},$$

$$(1b) \quad RCT = \sum_n (TC(hkl)_n \times \cos \alpha(hkl)_n),$$

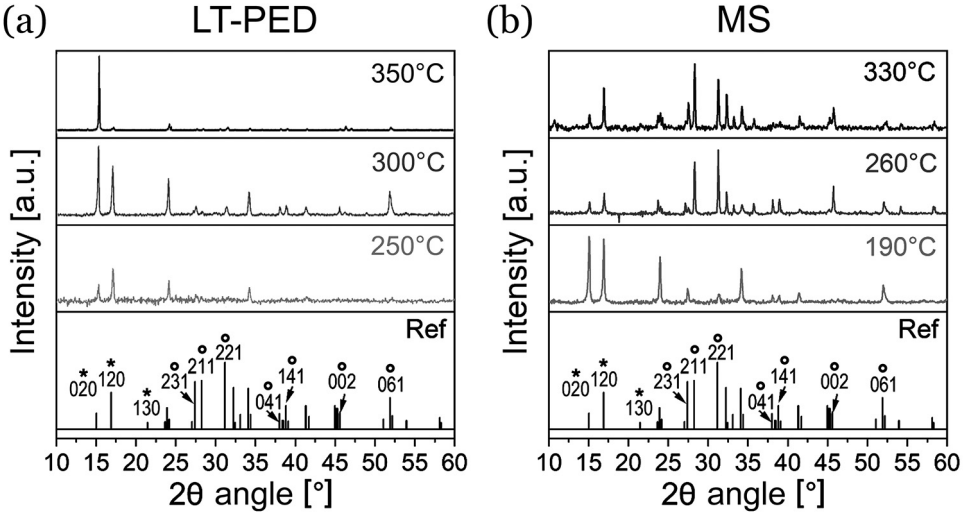


Fig. 2. – X-ray diffraction patterns of  $\text{Sb}_2\text{Se}_3$  films deposited at different temperatures on bare glass substrates: (a) by LT-PED; (b) by MS. JPCDS 15–0681 reference is reported at the bottom, where a few selected reflections are highlighted with \* symbol, if related to ribbons laying parallel to the substrates, or with  $\circ$  symbol, if related to ribbons with an orientation having a non-zero perpendicular component ( $hkl$  with  $l \neq 0$ ).

where  $I(hkl)$  is the relative intensity of the  $(hkl)$  peak in the collected XRD pattern and  $I_0(hkl)$  is the relative intensity for the same peak in the JCPDS 15–0681 reference; summation are calculated for  $n = 10$  reflections, chosen among the more intense ones that have been experimentally observed in the collected spectra and labeled in the reference pattern in fig. 2: (020), (120), (130), (231), (211), (221), (041), (141), (002) and (061);  $\alpha(hkl)$  is the angle between the ribbon axis and the normal to the surface for  $hkl$  orientation.

$TC(hkl)$  is the normalized “texture coefficient”, while  $RCT$  is the “ribbon carrier transport” coefficient. According to the definition, a preferential orientation of grains in ASe films along one of these directions is present when the corresponding  $RTC > 1$ ; so the larger is the  $RCT$  value, the better is the average preferential crystalline orientation of the  $\text{Sb}_2\text{Se}_3$  film.

The comparison of the obtained  $RCT$  values obtained for the different substrates, using both techniques at  $300^\circ\text{C}$ , is reported in fig. 3(a). While the best preferential orientation is achieved on FTO for LT-PED deposition, CdS provides the best result in the case of MS deposition. Good results are also obtained with ZnO, while Mo, which is often used in other cell structures reported in the literature, is the worst substrate for both techniques. As a general consideration, the plot in fig. 3(a) shows that MS deposition generally performs better than LT-PED. The details of XRD spectra of  $\text{Sb}_2\text{Se}_3$  films on CdS and Mo are reported in fig. 3(b) to highlight the differences.

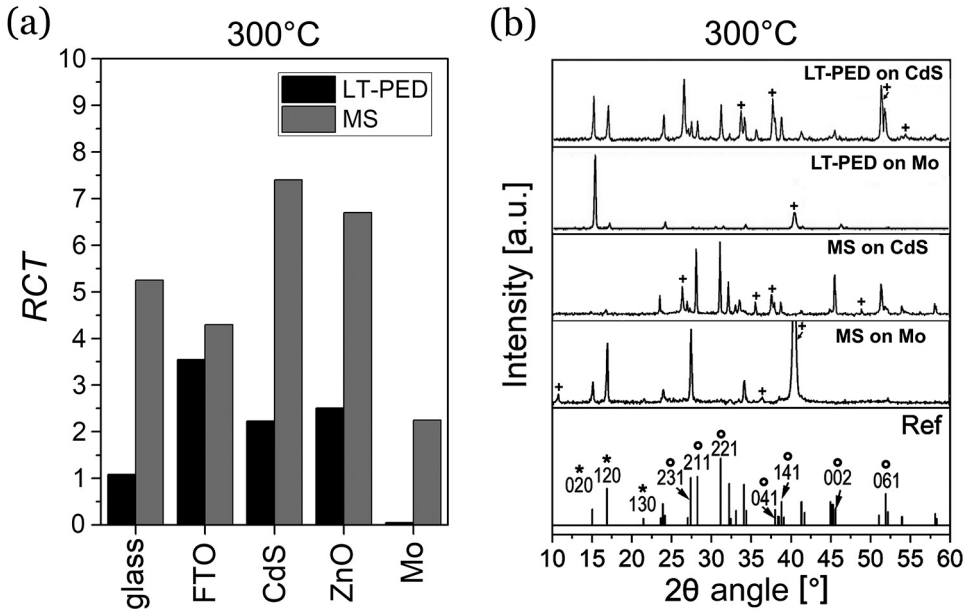


Fig. 3. – (a)  $RCT$  values for  $Sb_2Se_3$  films deposited on different substrates by LT-PED and MS at 300 °C. (b) X-ray diffraction patterns of  $Sb_2Se_3$  films deposited on Mo and CdS at 300 °C using LT-PED and MS; peaks from the used substrates are marked with + symbol; JPCDS 15–0681 reference is reported at the bottom, where a few selected reflections are highlighted with \* symbol, if related to ribbons laying parallel to the substrates, or with ° symbol, if related to ribbons with an orientation having a non-zero perpendicular component ( $hkl$  with  $l \neq 0$ ).

**3.3. Cell performance and Cu-doping.** – In order to confirm the correlation between the preferential crystalline orientation of grains in  $Sb_2Se_3$  films and the photovoltaic performance, complete cells were made with some of the samples that showed the best and the worst orientations: Mo and FTO by LT-PED deposition, as well as Mo, FTO and CdS by MS deposition (see refs. [9, 10] for details on cells production). The  $J$ - $V$  characteristics of these cell are reported in figs. 4(a) and (b) respectively.

From these plots it is easily visible that the cell performance is somehow proportional to the correct or uncorrect alignment of ribbons in the film (*i.e.*, proportional to the  $RCT$  value). Both cells with a  $Sb_2Se_3$  film deposited on Mo show very low short-circuit current density ( $J_{SC}$ ) values. The cell with a  $Sb_2Se_3$  film deposited by LT-PED on the FTO substrate has  $J_{SC} = 20.28 \text{ mA cm}^{-2}$ , open-circuit voltage ( $V_{OC}$ ) = 256 mV, fill factor (FF) = 39.2%, PCE = 2.1%. The cell with a  $Sb_2Se_3$  film deposited by MS on FTO substrate does not perform as well, having a poor FF, but the one on CdS substrate, that is related to the highest  $RCT$  value, has the best result:  $J_{SC} = 27.06 \text{ mA cm}^{-2}$ ,  $V_{OC} = 266 \text{ mV}$ , FF = 32.7%, PCE = 2.36%.

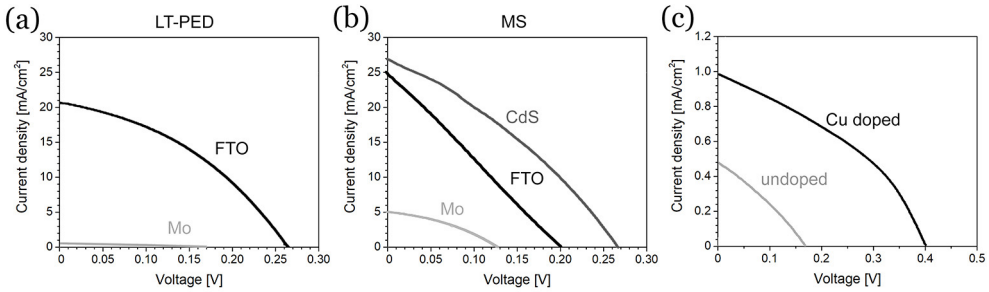


Fig. 4. – (a)  $J$ - $V$  plot for the two cells made with  $\text{Sb}_2\text{Se}_3$  films deposited by LT-PED:  $\text{ZnO:Al/ZnO/CdS}/(\text{Sb}_2\text{Se}_3/\text{Mo})/\text{glass}$  and  $\text{ZnO:Al/ZnO/CdS}/(\text{Sb}_2\text{Se}_3/\text{FTO})/\text{glass}$ . (b)  $J$ - $V$  plot for the three cells made with  $\text{Sb}_2\text{Se}_3$  films deposited by MS:  $\text{ZnO:Al/ZnO/CdS}/(\text{Sb}_2\text{Se}_3/\text{Mo})/\text{glass}$ ,  $\text{ZnO:Al/ZnO/CdS}/(\text{Sb}_2\text{Se}_3/\text{FTO})/\text{glass}$ , and superstrate  $\text{Au}/(\text{Sb}_2\text{Se}_3/\text{CdS})/\text{FTO}/\text{glass}$ . (c)  $J$ - $V$  plot for the undoped and the Cu-doped cells made with  $\text{Sb}_2\text{Se}_3$  films deposited by LT-PED.

All these results, however, are clearly affected by a very low  $V_{OC}$ . One of the possible explanation for such a low value may be found in the very low free charge-carrier density (namely as low as  $10^{13} \text{ cm}^{-3}$ ) that generally characterize  $\text{Sb}_2\text{Se}_3$  [5]. In order to proof this point, a Cu-doped  $\text{Sb}_2\text{Se}_3$  film was deposited on the Mo substrate by LT-PED, using a Cu-doped  $\text{Sb}_2\text{Se}_3$  target (custom synthesis). The preliminary result is shown in fig. 4(c) for the samples on the Mo substrate: thanks to the doping  $V_{OC}$  increases up to 0.4 V, nearly doubling the value of the undoped films.

#### 4. – Conclusions

Two industrial-production-oriented techniques, LT-PED and MS, have been tested for the deposition of  $\text{Sb}_2\text{Se}_3$  thin films for photovoltaic application. This study clearly demonstrates the importance of a “good” crystallographic orientation of  $\text{Sb}_2\text{Se}_3$  grains in the deposited films, avoiding  $(\text{Sb}_4\text{Se}_6)_n$  ribbons to lay on the same plane of the substrate, to build a working photovoltaic cell based on a  $\text{Sb}_2\text{Se}_3$  absorber. The best orientation in LT-PED and MS depositions, evaluated by means of their  $RCT$  values, have been respectively obtained on FTO and CdS substrates, heated at 300 °C. Despite the measured PCE values, that are the results of the contributions from all the cell layers and interfaces (to be optimized in the next future), the characterization of the cells, made with the deposited  $\text{Sb}_2\text{Se}_3$  films, clearly confirms the correlation between the cell performance and its average crystallographic orientation. Finally, the preliminary test of a cell, made with a Cu-doped  $\text{Sb}_2\text{Se}_3$  film, showed a possible way to improve the  $V_{OC}$  value in this kind of devices.

## REFERENCES

- [1] GREEN M. A., DUNLOP E., HOHL-EBINGER J., YOSHITA M., KOPIDAKIS N. and HAO X., *Prog. Photovolt.*, **29** (2021) 3.
- [2] NAIN P. and KUMAR A., *Renew. Sustain. Energy Rev.*, **119** (2020) 109592.
- [3] ANCTIL A. and FTHENAKIS V., *Prog. Photovolt.*, **21** (2013) 1253.
- [4] VADAPOO R., KRISHNAN S., YILMAZ H. and MARIN C., *Phys. Status Solidi B*, **248** (2011) 700.
- [5] MAVLONOV A., RAZYKOV T., RAZIQ F., GAN J., CHANTANA J., KAWANA Y., NISHIMURA T., WEI H., ZAKUTAYEV A. MINEMOTO T., ZU X., LI S. and QIAO L., *Sol. Energy*, **201** (2020) 227.
- [6] SHOCKLEY W. and QUEISSER H. J., *J. Appl. Phys.*, **32** (1961) 510.
- [7] CAO Y., ZHU X., JIANG J., LIU C., ZHOU J., NI J., ZHANG J. and PANG J., *Sol. Energy Mater. Sol. Cell.*, **26** (2020) 110279.
- [8] TANG R., *Nat. Energy*, **5** (2020) 587.
- [9] PATTINI F., RAMPINO S., MEZZADRI F., CALESTANI D., SPAGGIARI G., SIDOLI M., DELMONTE D., SALA A., GILIOLI E. and MAZZER M., *Sol. Energy Mater. Sol. Cell.*, **218** (2020) 110724.
- [10] SPAGGIARI G., PATTINI F., BERSANI D., CALESTANI D., DE IACOVO A., GILIOLI E., MEZZADRI F., SALA A., TREVISI G. and RAMPINO S., *J. Phys. D: Appl. Phys.*, **54** (2021) 385502.
- [11] RAMPINO S., PATTINI F., BRONZONI M., MAZZER M., SIDOLI M., SPAGGIARI S. and GILIOLI E., *Sol. Energy Mater. Sol. Cell.*, **185** (2018) 86.
- [12] CAVALLARI N., PATTINI F., RAMPINO S., ANNONI F., BAROZZI M., BRONZONI M., GILIOLI E., GOMBIA E., MARAGLIANO C., MAZZER M., PEPPONI G., SPAGGIARI G. and FORNARI R., *Appl. Surf. Sci.*, **412** (2017) 52.
- [13] MAZZER M., RAMPINO S., SPAGGIARI G., ANNONI F., BERSANI D., BISSOLI F., BRONZONI M., CALICCHIO M., GOMBIA E., KINGMA A., PATTINI F. and GILIOLI E., *Sol. Energy Mater. Sol. Cell.*, **166** (2017) 247.
- [14] BRONZONI M., STEFANCICH M. and RAMPINO S., *Thin Solid Films*, **520** (2012) 7054.